공학석사학위논문

2차원 착빙 해석자에 대한 표면 조도 모델의 확장

Extension of Surface Roughness Model for 2nd Generation Aircraft Icing code

2018년 2월

서울대학교 대학원

기계항공공학부

민 승 인

초 록

표면 조도는 착빙이 일어난 표면의 물리적 특성에 영향을 주기 때문에, 착빙 수치 해석 간에 중요하게 고려되어야 한다. 그러나 물리적 특성을 나타내는 모델을 사용하는 것은 수치 해석 방법에 적용하는 것이 복잡하기 때문에, 비교적 단순한 실험 결과에 기반한 선험적 경험식을 주로 사용하고 있다. 본 연구에서는 표면 조도의 물리적 특성을 나타내기 위해, 2세대 착빙 해석 코드에 확장된 표면 조도 모델을 적용하는 방법을 제시하였다. 해당 모델은 착빙 표면의 상태는 Bead, Rivulet, Water film의 3단계로 표면 위의 물의 양에 따라 구분하였으며, 각 상태를 나누는 기준점은 물에 작용하는 힘 평형 방정식을 토대로 계산하였다. 물의 양은 Water film을 고려하고 있는 지배방정식을 변형하여 1차 상미분방정식 형태로 나타내었다. 이러한 모델을 입증하기 위해서 다른 표면 조도 모델과 실험 결과에 대해서 표면 조도 높이, 열전도 계수, 그리고 형상에 대해서 비교하였다. 모델을 적용함에 따라서 표면 조도와 열전도 계수의 변화가 나타났지만, 형상의 경우 일부 조건에서는 개선된 결과를 나타내었다.

주요어 : 항공기 착빙, 표면 조도 모델, 대류 열전달

학 번 : 2016-20737

ABSTRACT

Extension of Surface Roughness Model for 2nd Generation Aircraft Icing Code

Seungin Min
Mechanical and Aerospace Engineering
The Graduate School
Seoul National University

Surface roughness should be taken into account when numerically predicting the aircraft icing shape since it affects the underlying physics of the frozen surface. However, empirical correlation equation based on experimental results has been widely used due to its simplicity and limitations of numerical methods for applying the physical model. To present the physical features of surface roughness, this paper proposes the extended roughness model implemented to the 2nd generation aircraft icing code based on the previously proposed analytical model. When applying the model, the analytical solution for the film thickness is derived based on modified governing equation. Then, through the force equilibrium equation, the maximum bead height and minimum film height are computed. Subsequently surface roughness and surface state are determined by comparing with the film thickness. For the verification of the model, the roughness height, heat convections and shapes were compared with

numerical results with other roughness models and experimental results. The changes in roughness height and heat convection were evident, but the shape was not significantly different from the numerical correlation results. Specifically, the reason for the change in roughness and heat convection is discussed. Finally the qualitative discussion is made for the little change in shape, and the necessity of the model was presented compared with the result of empirical correlation.

keywords : Aircraft Icing, Surface roughness, Convective heat transfer

***Student Number* : 2016-20737**

LIST

초 록 i

ABSTRACT ii

LIST iv

LIST OF FIGURES v

NOMENCLATURE 1

1. Introduction 3

2. Numerical Methodology 6

2.1 Aircraft icing code 7

2.2 Theoretical background for Surface roughness model 12

2.3 Previous surface roughness models 14

2.4 Present surface roughness model 18

3. Result and Discussion 25

3.1. Effect on heat convection 26

3.2 Ice shape verification – Fortin's model 28

3.3 Ice shape verification – NASA empirical correlation 33

3.4 Further studies 39

4. Conclusions 41

References 43

LIST OF FIGURES

FIGURE 1. MODULES OF THE AIRCRAFT ICING CODE 8

FIGURE 2. ICE SHAPE VARIATION DUE TO C_{CAL} 30

FIGURE 3. EFFECT OF C_{CAL} ON THE ROUGHNESS HEIGHT AND H_{CV} 32

FIGURE 4 ICE SHAPE UNDER DIFFERENT CONDITIONS 34

FIGURE 5. COMPARISON OF THE ROUGHNESS HEIGHT AND CONVECTION ENERGY DISTRIBUTION 36

FIGURE 6 ICE SHAPE COMPARISON AT DIFFERENT EMPIRICAL CORRELATION CONDITIONS 37

NOMENCLATURE

β	=	local collection efficiency
c	=	chord length, m
$C_{p,w}$	=	specific heat of water
$C_{p,i}$	=	specific heat of ice
D	=	single droplet diameter, m
Δt	=	exposed time in icing condition, s
$\vec{g}$	=	gravitational acceleration, 9.81 m/s^2
h	=	height, m
h_t	=	ice thickness, m
h_c	=	heat convection coefficient, W/m^2·K
h_f	=	height of water film, m
k_s	=	surface roughness height, m
L_{fus}	=	latent heat of fusion, 334 kJ/kg
LWC	=	liquid water contents, g/m^3
MVD	=	median volumetric droplet diameter, μm
$\dot{m}_{com}$	=	impinging water rate, kg/s
$\dot{m}_{ice}$	=	accumulated ice rate, kg/s
$\dot{m}_{eva}$	=	evaporating mass rate, kg/s
$\dot{e}_{com}$	=	impinging water energy rate, W/m^{2}s
$\dot{e}_{ice}$	=	accumulated ice energy rate, W/m^{2}s
$\dot{e}_{eva}$	=	evaporating energy rate, W/m^{2}s
$\dot{e}_{conv}$	=	convective energy rate, W/m^{2}s
μ	=	viscosity, Pa·s
p	=	pressure, Pa
ρ	=	density, g/m^3
s	=	length of wrap-around direction, m
σ	=	surface tension, N/m
t_{ice}	=	exposure time in icing conditions, s
t_m	=	total time to reach the mission altitude, s
T_∞	=	freestream temperature, K
$\tilde{T}_{eq}$	=	equilibrium temperature, ℃
$\vec{\tau}_{wall}$	=	shear stress on the water film from air, Pa

$\vec{u}$	=	velocity vector, m/s
$\overline{U}_f$	=	mean velocity of water film, m/s
V_∞	=	freestream velocity, m/s
e_f	=	analytical film height, m
$e_{f,min}$	=	analytical minimum film height, m
e_b	=	analytical bead height, m
R_g	=	non-dimensional gravitational ratio
R_w	=	non-dimensional aerodynamic flow ratio
θ_c	=	average contact angle, rad
F_σ	=	surface tension force, N
F_p	=	aerodynamic pressure force, N
F_d	=	aerodynamic drag force, N
F_g	=	gravitational force, N
k_m	=	non-dimensional mass flow rate coefficient
k_{vel}	=	non-dimensional film velocity coefficient
d_{wall}	=	wall distance, m
d_{new}	=	modified roughness wall distance, m
k_{eff}	=	effective thermal conductivity, W/m°C
k_T	=	turbulent thermal conductivity, W/m°C
k	=	thermal conductivity, W/m°C
R_g	=	non-dimensional gravitational ratio
Re	=	Reynolds number

Sub

a	=	air properties
d	=	droplet properties
i	=	ice properties
ice	=	properties of surfaces with ice accumulation
∞	=	freestream
w	=	water properties
$bead$	=	Bead properties

1. Introduction

An aircraft icing simulation iteratively predicts the final ice shape when an aircraft is exposed to icing conditions. Such a simulation is composed of four modules: aerodynamic, droplet trajectory, thermodynamic, and mesh generation modules. Specifically, the thermodynamic module computes the ice accretion rate by solving the continuity and energy balance equations of the water film on the surface.

When a water droplet freezes, it changes the surface roughness, thereby affecting the thermal gradient, which is responsible for the convective heat transfer and eventually associated with the final ice formation. To consider the effects of surface roughness, most icing simulations use a representative uniform value obtained from numerical modeling. In the early numerical simulations, the surface roughness value used in the integral boundary layer equation was defined by the users to estimate the ice shape as in experiments[1]. Because of the absence of a quantitative correlation between the roughness elements, an empirical correlation based on the experimental results with respect to the velocity, temperature, and liquid water content (LWC) was adopted, which provided the linear relation for each parameter[2]. Though the correlation yields the equivalent roughness height according to the test conditions, the empirical modeling is associated with several problems. First, an empirical approach does not simulate the physics of the surface roughness, but only presents the numerical results. Moreover, because the surface roughness is modeled based on several experimental results, it is not appropriate for conditions beyond the scope of the model.

Since the mid-1980s, studies indicating the necessity of considering the surface roughness in ice accretion prediction have been the focus of much research To increase the understanding of the surface roughness due to icing, Olsen[3] observed the surface flow of a water film on an airfoil surface through enlarged movies and photographs. The author identified a transient water film movement at the starting point, affecting the local roughness, and in turn, changing the final ice shape. Hansman[4] conducted a series of experiments focusing on the physics of the unfrozen water during glazed-ice accretion. He provided qualitative results of the ice shape on cylinders with different roughness, indicating that the roughness had an impact on the ice shape. Shin[5] also investigated the effect of icing parameters on the ice accretion process by a quantitative measurement of the roughness.

Some studies have been conducted to numerically model the changes in the surface roughness. Fortin[7] proposed a new methodology to model the physics of a water film and applied it to the panel method for aircraft icing simulation. He simulated the local roughness and heat transfer coefficient by introducing a new analytical model. However, his model could be applied only to the panel method, and thus, presented a low fidelity. Therefore, to compensate this, an arbitrary parameter is used to match the shape shown in the experiment. Croce[8] conducted two numerical studies. In the first, he used only the bead height on the surface to predict the final ice shape. In the second study, the surface roughness of a plate was calculated using the Lagrangian method by tracking each droplet.

However, previous models have several ambiguities. The NASA empirical correlation was based on limited experiments and provided inexact results under other conditions. In addition, because of the uniform application of a

constant value to the surface, the correlation could not classify the physical characteristics into those of a water bead, rivulet, and film. The model by Fortin suggested considering the physical properties, but the arbitrariness according to the fidelity of the model could lead to crude numerical results in the absence of a specific experimental result. Croce demonstrated that a beading on a surface could be used as an approach for extending the roughness model to an icing code based on the Navier–Stokes equation[8].

This study employs an advanced surface roughness model, and the effect of its application is determined by comparing it with other models. The primary objective of this study is to reduce the arbitrariness of a previously used roughness model while expanding the model to a Navier–Stokes-based aircraft icing code. First, the local surface roughness is computed without arbitrariness by applying the analytical solution of the modified governing equation. Second, considering the force equilibrium at the surface, the ice shape is reasonably predicted beyond the conditions under which the empirical correlation is formulated.

2. Numerical Methodology

Aircraft icing is a serious threat to the aviation safety since it causes the significant change in shapes of fuselage, wings, and engine nacelle through the accumulated ice and the malfunction of measuring equipment. Particularly, the shape deformation of the wings causes the degradation of the aerodynamic performance such as the decrease of lift and the increase of drag. Therefore, it is imperative accurately predicting the shape change due to the aircraft icing. Recently, the advanced computing technology made possible the prediction of the ice accretion shapes and its aerodynamic performance using numerical simulation.

In applying the numerical analysis, it is necessary to simulate the physical features of the aircraft icing including the aerodynamics, movements of the water droplets, and the thermodynamic phenomena occurring on the aircraft surface. Among these features, the heat transfer, which describes the energy exchange at the surface, is directly related to the ice accretion. Since the latent heat released by the phase transition of the water into ice is balanced off by the heat convection, thus prediction of the heat convection rate is important factor in calculating the amount and the shape of ice accurately.

2.1 Aircraft icing code

The aircraft icing code, as shown in Fig. 1, consists of four modules. Each module sequentially computes the aerodynamic force, droplet trajectory, thermodynamics, and shape deformation. Though aircraft icing is an inherently unsteady phenomenon lasting from a few to tens of minutes, a quasi-steady state is assumed for computational efficiency. The aircraft icing code, as shown in Fig. 1, consists of four modules. Each module sequentially computes the aerodynamic force, droplet trajectory, thermodynamics, and shape deformation. Though aircraft icing is an inherently unsteady phenomenon lasting from a few to tens of minutes, a quasi-steady state is assumed for computational efficiency. To consider the impact of shape change due to icing, a multi-shot method that divides the total icing time into several steps to account for the ice accretion as a function of time is used.

The first computer program for ice shape prediction was to predict the 2D ice shape on the airfoil and its aerodynamic performance based on the inviscid and incompressible 2D Panel method. Subsequent programs are based on Panel code as proposed by NASA, and these codes are generally defined as first generation aircraft icing code. The first generation icing code has the following characteristics. . Since It used inviscid and incompressible aerodynamic solvers such as panel method, to consider the viscosity effect and the heat transfer effect on the surface, IBL(Interactive Boundary Layer) and Reynolds analogy were adopted for the extension of the icing code. The Lagrangian approach was employed for the droplet-trajectory calculation module. To compute the ice shape 2D Messinger model [12] is used for the thermodynamic module.

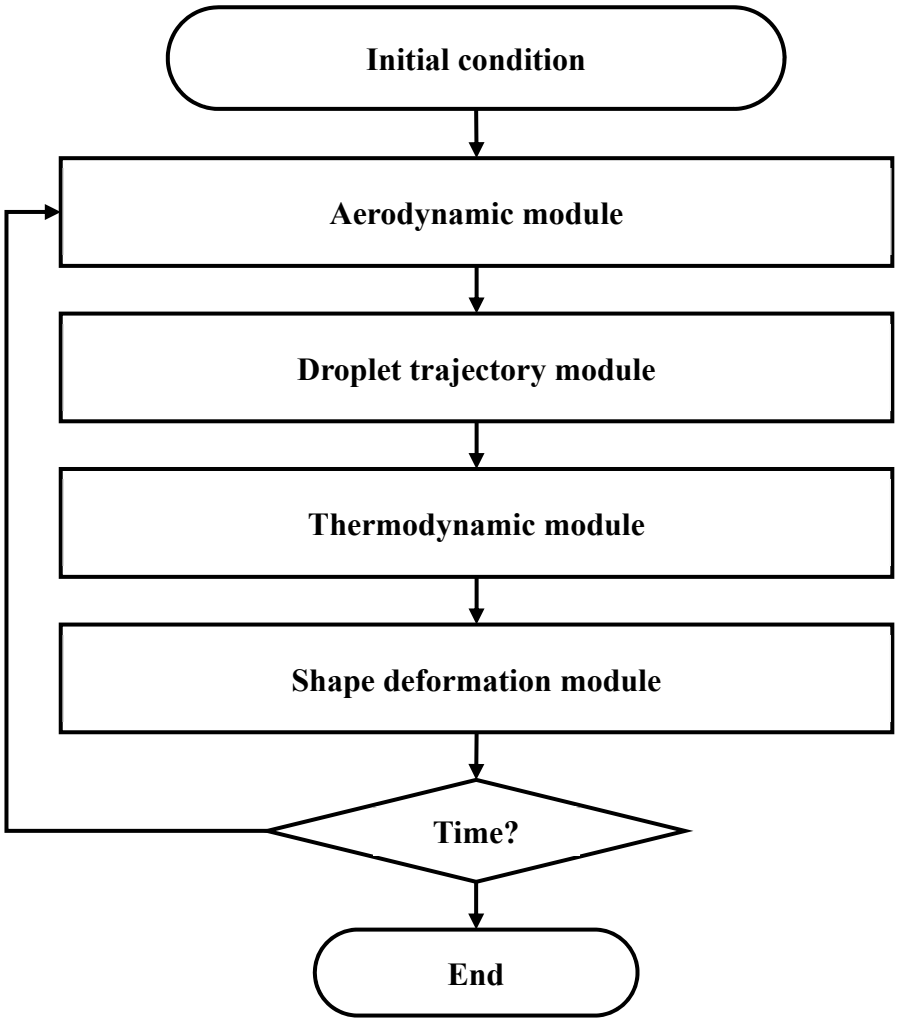

Figure 1. Modules of the aircraft icing code

Though the first generation icing code provided the efficient tool for predicting the ice shape, there are several limitations. First, since the code is based on the inviscid aerodynamic solver, the flow separation which affects the droplet trajectory and aerodynamic performance is not properly captured. Also, since the code is developed for 2D, the icing on generic 3D features such as fuselage and wing span is restrictedly computed.

With the advance in the computing technology, the aircraft icing codes based on Navier-Stokes equation were developed and classified into second generation aircraft icing code. These type of codes applied 3D Eulerian approach for the droplet-trajectory calculation module. To handle the movement of the water film on the surface with consideration of 3D movement, the modified water film equation based on Messinger model was included. The difference between first and second generation code is shown in Table 1.

Table 1. Comparison of 1st and 2nd generation aircraft icing code

	1st generation codes LEWICE(NASA)	**2nd generation codes FENSAP-ICE**
Period	1980 ~ 1990s	1990s ~
Aerodynamic module	Panel method, Euler equation	Navier – Stokes equation
Droplet Tajectory module	Lagrangian approach	Eulerian approach
Thermodnamic module	2D Messinger model	Thin water film model (Extended messenger)
Features	✓ Boundary layer theory ✓ Reynolds analogy for heat transfer	✓ Consider the water film movement on surface

In this study, the surface roughness model is extended to a Reynolds-averaged Navier–Stokes(RANS)-based code to completely take into consideration both the surface roughness and surface state. The model is built in OpenFOAM^{TM} [9], an open source code. The unsteady compressible Reynolds-averaged Navier–Stokes (RANS) equation is applied in the aerodynamic solver. In the case of turbulent closure, the roughness-modified Spalart–Allmaras[10] model is used to deal with the surface roughness of the iced surface.

The droplet trajectory module calculates the collection efficiency on the surface. By representing the droplets in a finite volume using droplet density, the continuity and momentum equations for a droplet are calculated using the velocity vectors from the aerodynamic solver as expressed in eqs. (1) and (2) [11].

$$\frac{\partial \rho_d}{\partial t} + \nabla \cdot (\rho_d \overline{U}_d) = 0 \tag{1}$$

$$\frac{\partial \rho_d \overline{U}_d}{\partial t} + \nabla(\rho_d \overline{U}_d \overline{U}_d) = \frac{3}{4}\frac{\rho_d \mu_a C_D Re_d}{\rho_w MVD^2}(\overline{U}_a - \overline{U}_d) + \rho_d g\left(1 - \frac{\rho_a}{\rho_w}\right) \tag{2}$$

Collection efficiency, β, representing the flux of a droplet on the surface is computed with the surface normal vector of the droplet and droplet density using eq. (3) [11].

$$\beta = \frac{\rho_d \ \overline{U}_{d,n}}{LWC_\infty \cdot U_\infty} \tag{3}$$

The thermodynamic solver is a module for calculating the ice accretion rate using a three-dimensional Eulerian thin-water film model extended from the two-dimensional Messinger model[12]. The model consists of a set of two equations, namely, the continuity and energy conservation equations, defined below[11].

$$\rho_w \left[\frac{\partial \mathrm{h}_f}{\partial \mathrm{t}} + \nabla \cdot \left(\mathrm{h}_f \overline{U}_f \right) \right] = \dot{m}_{imp} - \dot{m}_{ice} - \dot{m}_{eva} \tag{4}$$

$$\rho_w \left[\frac{\partial \mathrm{h}_f c_{p,w} T_c}{\partial \mathrm{t}} + \nabla \cdot \left(\mathrm{h}_f c_{p,w} T_c \overline{U}_f \right) \right] = \dot{e}_{imp} + \dot{e}_{ice} - \dot{e}_{eva} - \dot{e}_{conv} \tag{5}$$

Since there are three unknowns in the two equations, a compatibility relation assuming one unknown value according to the ice accretion type is necessary. The aerodynamic solver, turbulent model, and droplet trajectory solver are validated. A detailed description of this method can be found in the work by Son et. al[11]. The ice thickness for each step is computed, and the surface mesh is protruded. The process for each calculation step is repeated for the entire icing exposure time.

2.2 Theoretical background for Surface roughness model

While aircraft icing is a severe risk to aviation safety, there are still limited models of predicting ice accretion shapes. Surface roughness is one of these limitations based on empirical sand grain roughness model from NASA. The surface roughness, not only related to the skin friction penalty, however, increased roughness could enhance the convective and evaporative heat fluxes and accelerate the freezing rate of run-back water affecting ice shape generation. Experimental evidence shows that water flow over the surface could form different types of surface, usually classified into beads, rivulets, and film, and create significant surface roughness. Thus, there are growing interests in numerical analysis of surface roughness distribution during the CFD-Icing simulation procedure.

Herein, the surface roughness model assumes that the surface state is classified by the amount of the water on the surface. In the initial stage of icing, the attached droplets are distributed on the surface as beads. As icing proceeds, the number of droplets on the surface increases, and the neighboring droplets coalesce to form a larger bead. Next, the beads grow and begin to move when they reach a certain size, so that a runback flow, such as a rivulet and film, occurs on the surface. This change in the surface due to an increase in the amount of water on the surface has been shown experimentally.

To apply the surface roughness model based on the water film physics, it is required to understand the relationship between the water behavior and the surface state. Quantitative analysis of water mass and water behavior on the surface were conducted through the experiment by Beysen[6]. The surface

roughness by water droplet on the surface appears in his study[6]. He investigated this growth of water beads through experiments on surface coverage, which presents the water mass on the surface. For the surface coverage under 30% where condensation mainly occurs, after droplets impact on the surface, they statistically spread over the surface, and nucleation starts inside the water droplet. When surface coverage is 30 ~ 85%, coalescence of neighboring beads take place, and for empty area after the coalescence new droplet impinges. After the surface coverage reaches 80 ~ 90%, the beads grow up to maximum size and runback starts.

Beysen[6] investigated the above-mentioned growth of a bead via experiments on surface coverage, which presented the water mass on the surface. The concept was proposed by Fortin[7] and divides the surface state into a (1) film, (2) rivulet, and (3) bead state depending on the amount of water on the local surface. In a film state, the entire surface is covered with flowing shallow water. For a rivulet, in contrast with a film, some of the water flows and some does not, forming a stream on the surface. The bead state is the stationary state where the impinging droplets form the beads and grow. Each state is distinguished with respect to the amount of water on the surface or the film thickness per unit area.

2.3 Previous surface roughness models

Modeling of the surface roughness due to ice accretion has been studied since the 90's. The NASA LEWICE tried the empirical correlation obtained by parametric studies from experimental results[2]. The surface roughness values can be estimated a function of velocity, temperature, and LWC.

$$\left[\frac{k_s/C}{k_s/C_{base}}\right]_{V_\infty} = 0.4286 + 0.0044V_\infty \tag{6}$$

$$\left[\frac{k_s/C}{k_s/C_{base}}\right]_{LWC} = 0.5714 + 0.2457LWC + 1.2571LWC^2 \tag{7}$$

$$\left[\frac{k_s/C}{k_s/C_{base}}\right]_{T_\infty} = 46.8384\left(\frac{T_\infty}{1000}\right) - 11.2037 \tag{8}$$

$$k_s = \left[\frac{\frac{k_s}{C}}{\frac{k_s}{C_{base}}}\right]_{V_\infty}\left[\frac{\frac{k_s}{C}}{\frac{k_s}{C_{base}}}\right]_{LWC}\left[\frac{\frac{k_s}{C}}{\frac{k_s}{C_{base}}}\right]_{T_\infty}\left(\frac{k_s}{c_{base}}\right)c \tag{9}$$

However, this simple modeling involves several problems. First, the empirical approach does not simulate the roughness distribution, but single value. Second, since it is correlated by using limited cases of experimental results, the range of applicable variables such as velocity, temperature, and LWC is also restricted. For those reasons, it is necessary to apply the physical roughness model, which can model the physical characteristics of the iced

surface rather than the empirical correlation.

The analytical model presented the observations and conclusions made from experiment that impinging water droplets freeze on impact and forms the rough surface. When the impinging droplet increases with the temperature near freezing point, glaze surface where smooth surface is made. To represent these alternatives, Fortin[7] developed the analytical formulations assuming the liquid water mass on surface to be in a film, rivulet, and bead. The object of the model is to determine the transient convective heat transfer coefficient during ice accretion. The ice shpaes are predicted using the 2D CIRAMIL code[7], which is the 1st generation aircraft icing code based on the panel method.

To compute the film height, the analytical model introduced by Al-Khalil et al.[14] in de-icing simulations is used, since the panel method used for the roughness model application and film height is not considered as shown in eq. (10). The roughness height is considered to be equal to the wave height as in eq. (11).

$$e_f = \sqrt{\frac{2}{\tau_w}} \sqrt{\frac{\mu_w \ m_w}{\rho_w \ \Delta b \ \Delta t}} \ C_{cal} \tag{10}$$

$$k_s = \frac{3}{4} \ \frac{\tau_w}{\mu_w} \ \sqrt{\frac{{e_f}^3}{g}} \tag{11}$$

When the water film height exceeds the minimum film height, the surface water forms a film as mentioned above. The minimum film height is computed through multiplying shape factor to the bead height as follows.

$$e_{f,min} = \sqrt{\frac{\theta_c - \sin(\theta_c)\cos(\theta_c)}{2\ \sin(\theta_c)}}\ e_b \tag{12}$$

Bead height is computed through the analytical model derived from following force equilibrium equation.

$$\pm F_g \pm F_w - F_\sigma = 0 \tag{13}$$

Assuming that a component of force acting parallel to the surface moves the bead, the height of the bead is given by:

$$e_b = \frac{-R_w\ C_G(e_b) + \sqrt{{R_w}^2 {C_G}^2(e_b) + 4R_g\Delta\theta_c}}{2\ R_g} \tag{14}$$

$$R_g = \frac{2}{3}\ g\frac{\rho_w}{\sigma_w}\ \left[\frac{2+\cos(\theta_c)}{2\ R_g}\right]\sin(\theta_c) \tag{15}$$

$$R_w = \frac{2}{\pi}\ \frac{\tau_w}{\sigma_w}\ \frac{\theta_c - \sin(\theta_c)\cos(\theta_c)}{\sin(\theta_c)^2\ \ [1-\cos(\theta_c)]} \tag{16}$$

R_g and R_w represent the gravitational ratio and aerodynamic flow ratio which

are projection of gravitational and aerodynamic force parallel to the surface divided by the rigidity force, respectively.

For the rivulet state, Fortin [7] assumed that when the surface is exposed to the droplet impingement, all the beads would starts to flow forming the rivulet. . A detailed description of this method can be found in the work by Fortin [7].

2.4 Present surface roughness model

The concept was proposed by Fortin[7] and divides the surface state into a (1) water film, (2) rivulet, and (3) bead state depending on the amount of water on the local surface. In this study, in order to apply this concept to the RANS equation based code, the amount of water was calculated through film thickness and the roughness height was computed through the force equation acting on each state.

1) Water film

When the impinging water mass is larger than the accreting ice, the remaining water on the surface increases and forms a water film. The film thickness appears to be associated with the governing equations of the current thermodynamic module. However, because a quasi-steady state assumption is applied to the solver, the initial film thickness is assumed as an unsteady parameter. Therefore, in this study, a new analytical solution of film thickness is derived based on certain assumptions applied to the governing equation of the thermodynamic model. The assumptions applied are as follows:

(1) The convection term of the governing equation can be split into run-in and run-out water mass.
(2) Ice and water only coexist at surface temperature $T_{sur} = 0\ °\mathrm{C}$.

Applying the first assumption, the convection term $\rho_w \nabla \cdot \left(\mathrm{h}_f \overline{U}_f\right)$ in the continuity equation of the thermodynamic module is divided into run-in and

run-out water mass. The run-in water mass is treated as a source term, and the run-out water is expressed as the product of the film thickness and velocity as expressed in eq. (17). Applying this to the continuity equation, eq. (4) is converted into the form of a first-order ordinary differential equation for the film thickness, as given in eq. (18).

$$\dot{m}_{out} = \frac{\bar{\tau}}{2\mu_w} {h_f}^2 \tag{17}$$

$$\frac{\partial \mathrm{h}_f}{\partial \mathrm{t}} + \frac{\bar{\tau}}{2\mu_w} {h_f}^2 = (\dot{m}_{com} + \dot{m}_{in} - \dot{m}_{ice} - \dot{m}_{eva}) \tag{18}$$

The second assumption simplifies the energy equation of the governing equation. Because it is assumed that the water film exists only at the freezing temperature, eq. (5). becomes eq. (19) when no terms are related to the film thickness.

$$0 = \dot{m}_{com}\left[c_{p,w}\tilde{T}_{d,\infty} + \frac{1}{2}U_d^2\right] + \dot{m}_{ice}\left[L_{fus}\right] - L_{eva}\dot{m}_{eva} + h_c(T_c - T_\infty) \tag{19}$$

As the term related to a film does not appear in the energy conservation, the analytical solution of the modified mass conservation equation yields the film thickness. Constant k_m is a mass coefficient, which is the right-hand side term in eq. (21), and constant k_{vel} is the film velocity coefficient expressed as $\frac{\bar{\tau}}{2\mu_w}$.

$$h_f = \frac{\sqrt{k_m}\tanh(\sqrt{k_{vel}}\sqrt{k_m}t)}{\sqrt{k_{vel}}} \tag{20}$$

$$k_m = \frac{1}{\rho_w}(\dot{m}_{com} + \dot{m}_{in} - \dot{m}_{ice} - \dot{m}_{eva}) \tag{21}$$

2) Rivulet

When the water film diminishes, the momentum of the film driving the flow cannot overcome the surface tension. Then, the film splits and flows into the rivulet. Therefore, the criterion separating a film and rivulet can be defined by solving the force equilibrium equation immediately before the film splits into the rivulet.

As the surface flow starts, the kinetic energy of the film acts as a pressure force at the interface between the surface and film, and becomes an external force that drives the film flow. When the external force is larger than the surface tension acting on the film, the film remains intact; however, with the loss of momentum, the film flow splits into the rivulet. The surface tension and external force acting on the film are defined by eqs. (22) and (23).

$$F_\sigma = \sigma_w[1 - \cos(\theta_{avg})] \tag{22}$$

$$F_p = \int \frac{1}{2}\rho[\frac{\tau_w}{\mu_w}y - \frac{y^2}{\mu_w}\left(\frac{dp}{dx} + \rho g\right)]^2 \; d\,y \tag{23}$$

Based on the minimum film height, if the calculated film thickness decreases, it is assumed to be a rivulet. Then, the surface roughness height is the maximum bead height.

3) Bead

At the start of icing formation, the droplets are scattered on the surface and grow into beads. The beads on the surface are assumed to be subjected to gravitational and aerodynamic forces acting as the external force, with the surface tension acting as the as reacting force. Each component is shown in eqs. (24)–(27).

$$\overrightarrow{F_\sigma} = \int_0^\pi \sigma_w \cos\big(\theta(\varphi)\big) \cos(\varphi)\, \mathrm{r}_{bead} d\varphi \tag{24}$$

$$\overrightarrow{F_g} = \rho_{bead} g_i V_{bead} \tag{25}$$

$$\overrightarrow{F_d} = \int \tau_w(s) ds \tag{26}$$

$$\overrightarrow{F_p} = \int \frac{dp}{dx_i}\ dV \tag{27}$$

When a bead grows, the forces are in equilibrium, but when it exceeds a particular size, the external force becomes larger and it flows into the rivulet. The maximum height for the bead growth is computed from the equilibrium state instantaneously before the motion. If the remaining water mass is less than the mass when the surface coverage with the beads is maximum, the surface is a bead. The height of the bead is the ratio of the remaining water mass to the maximum bead height.

Surface roughness transition due to ice accretion induces the changes of

viscous effect associated relative motion between the fluid and the surface. As the aerodynamic solver is based on RANS equation which is focusing on the mean flow properties, application of adequate turbulence model which can consider the effect of roughness is needed.

For the present study, Spalart-Allmaras model with wall roughness correction is used [10]. This model uses the same governing equation with standard Spalart-Allmaras model, but modifies wall distance and boundary condition to account for enhanced turbulent effect by surface roughness. Through this turbulent model, the impact of the surface roughness model on heat convection is presented and affect the final ice shape.

In this paper, since the roughness is not a single value but a distribution, modification is necessary for the turbulence model. The wall distance which represents distance from the control volume to nearest wall is expressed as

$$d_{new}(s) = d_{wall} + 0.03k_s(s) \tag{28}$$

where $d_{new}(s)$ is modified wall distance and $k_s(s)$ is roughness height. Since roughness is a distribution, $k_s(s)$ is differed along the surface boundary. For the outer boundary region, it is assumed that the effect of roughness is averaged. The boundary condition $\hat{v}_{wall} = 0$ is modified as eq. (29).

$$\frac{\partial \tilde{v}}{\partial n} = \frac{\tilde{v}}{d_{new}(s)} \tag{29}$$

For every time step, roughness height is recalculated according to the shape

deformation and change of the surface state, modified wall distance and the boundary condition is applied to the aerodynamic solver to take account of the newly predicted surface roughness.

The current model applied to the 2nd generation icing code differs from the model G. Fortin applied to the 1st generation code.

(1) The first is due to the difference in the aerodynamic solver on which each code is based. Unlike the Navier-stokes equation, which is used for 2nd generation code, the 1st generation code uses the panel method of Euler equation, so it does not provide all the parameters needed for force equilibrium equation at the surface such as wall shear stress. Therefore, to consider these values additionally, an analytical model such as boundary layer theory is used which lowers the fidelity of the solver. For accuracy, Fortin [7] applied a calibration parameter to the analytical solution to correct the predicted roughness height by matching the numerically calculated ice shape to experimental result. This method can apply different calibration parameters depending on the analysis conditions, resulting in arbitrariness of the results.

(2) The second is the difference in method to calculate the film height, which is an important parameter of the roughness model. Current numerical method considers the film height through the governing equation as show in eq. (4) and eq. (5). Based on this, physics based film height is derived through the 1st ODE assumptions. On the other hand, G. Fortin's model was applied to the Messinger model without consideration of film height, so additional analytical solution for film height is introduced. Therefore, the calibration parameter were applied for correction of the solution as appears above.

(3) The third is how to reflect the impact of roughness in aircraft icing process.

This is also related to the aerodynamic solver difference mentioned above. The present RANS based 2nd generation code enhances the heat convection characteristics by considering the influence of roughness in the turbulence model. Fortin [7], on the other hand, described the Stanton number as a function of friction coefficient for a rough plate in turbulent regime defined by Spalding analogy [7]. The differences are discussed later in the Result & Discussion section.

In this study, the physical roughness method applied to the 1st generation aircraft icing code is extended to the 2nd generation code. For the analytical solution used in the existing model, arbitrariness of the solution is removed by applying the model based on governing equations. Also, by deriving the analytical solution for film height through the 1st ODE assumption, the limited expandability by the quasi-steady state assumptions applied to the present numerical method has been overcome.

3. Result and Discussion

In this section, the results of the simulation with current surface roughness model applied are compared with those of empirical correlation and Fortin's roughness model. First, the effect of calibration parameter(C_{cal}) of the Fortin's model is investigated, and the difference between the model and current model were compared. Next, the surface roughness height, heat convection coefficient(h_{cv}) and ice shapes with current surface roughness model applied are compared with those of empirical correlation.

3.1. Effect on heat convection

During the ice accretion, heat transfer at the surface is taken account to determine the ice accretion rate and the surface temperature. Assuming the steady state for the quasi steady energy equation expressed in eq. (31), it can be expressed in terms of the sum of energy on the control volume.

$$\dot{e}_{imp} + \dot{e}_{in} = \dot{e}_{ice} + \dot{e}_{out} + \dot{e}_{conv} + \dot{e}_{evap} \tag{31}$$

When the water freezes, given off energy for the phase transition of liquid to solid is the main source of energy income and appears to be product of latent heat and ice accretion rate. Then, generated heat by this phase transition is released into the air by evaporation or heat convection. Therefore, the heat convection rate is directly related to the calculation of ice accretion rate and it is important to measure accurately.

Characterized by temperature gradient and heat flux, heat convection is a consequence of temperature difference between the surface and fluid. Since phase transition of water into ice occurs at freezing temperature at 273.15K, there is a distribution ranging from the freezing temperature to the ambient temperature depending on the state of the surface, and thus the temperature gradient appears to forming thermal boundary layer. Through this region, the heat generated by the solidification and impingement of droplet is transferred to the freestream region. There are mainly two aspects of motion of the heat transfer; specific molecular motion defined by fluid properties and bulk, macroscopic fluid motion mainly affected by flow properties which highly

affects for the turbulent region. When the ice accreted on the surface, the flow becomes fully turbulent, and therefore both aspects of heat transfer should be considered.

In this paper, to simulate the turbulent flow, RANS equation and turbulent model is used. For the numerical calculation, the heat transfer rate is expressed in terms of the effective thermal conductivity k_{eff} and the temperature gradient as shown in eq. (32).

$$\vec{q} = k_{eff}\nabla T = (k + k_T)\nabla T \tag{32}$$

The effective thermal conductivity is the sum of thermal conductivity and turbulent thermal conductivity which is calculated from the turbulent model. As mentioned previously, roughness modified Spalart-Allmaras[10] is used to take account of the effect of the surface roughness.

Considering the Reynolds analogy that describe the physical mechanism for the heat transfer in a turbulent boundary layer, surface roughness is important parameter for heat convection coefficient. The decrease in the surface roughness size leads to an increase in the thickness of the boundary layer due to the loss of the turbulence effect, which results in a decline in the temperature gradient inside the boundary layer and also a decrease in the heat convection coefficient.

3.2 Ice shape verification – Fortin's model

Table 2 presents the verification conditions for comparing the results of the current and previous models. As can be seen from Table 2, the conditions are classified into glaze and rime conditions based on the temperature. In the glaze condition, the ambient temperature is near the freezing point, and, therefore, water and ice appear together. In the case of rime condition, the temperature is very low and impinging droplets freeze immediately. Because the ice shape differs depending on the conditions, two different cases are investigated to observe the changes when different surface roughness models are applied.

Table 2. Verification conditions

	Glaze	Rime
Airfoil	NACA0012	NACA0012
α [˚]	4	4
V_∞ [m/s]	67.05	67.05
T_∞ [°C]	-4.4	-28.3
LWC [g/m³]	1.0	1.0
MVD [μm]	20	20

※ LWC = Liquid Water Contents
※ MVD = Median Volume Diameter

The final ice shapes for both the roughness models are depicted in Fig 2. Fig 2(a) shows the result of applying the C_{cal} of Fortin's model to the glaze case and the results of the current model and experiments. In this figure, though the conditions are not changed, the final ice shapes appear to vary with the C_{cal} of Fortin's model. The surface roughness and h_{cv} increase with C_{cal}. With the

increment in heat convection, the amount of freezing ice also increases, which reduces the amount of water flowing out from the stagnation point and results in the concentration of ice near the stagnation point. In Fig 2(a), when C_{cal} is 10, ice is barely accumulates at the stagnation point, though it grows thick toward the trailing edge. In contrast, when C_{cal} is 50 and 100, the ice is thick at the stagnation point and the ice horn does not appear because of less water flowing backward. As shown above, for Fortin's model, the ice shape is highly dependent on C_{cal}, and if the experimental results are not obtained under certain conditions, then it is difficult to make accurate predictions using this model.

Fig 2(b) presents the effect of using the C_{cal} of Fortin's model for the rime case. In contrast with Fig 2(a), all the results exhibit a similar ice shape in Fig 2(b). In the rime case, most droplets freeze owing to the low temperature and there is a slight backward water flow. Therefore, for the rime case, the shape difference is less because the change in C_{cal} does not affect the ice accretion rate.

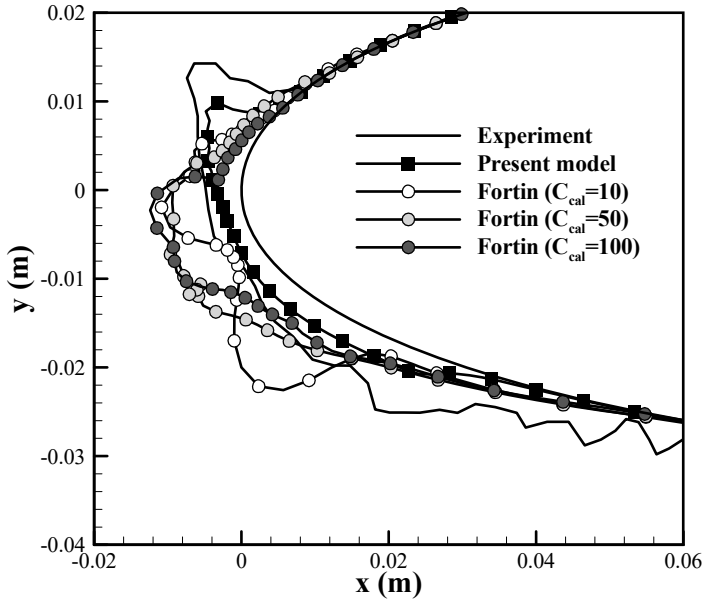

(a) Glaze case

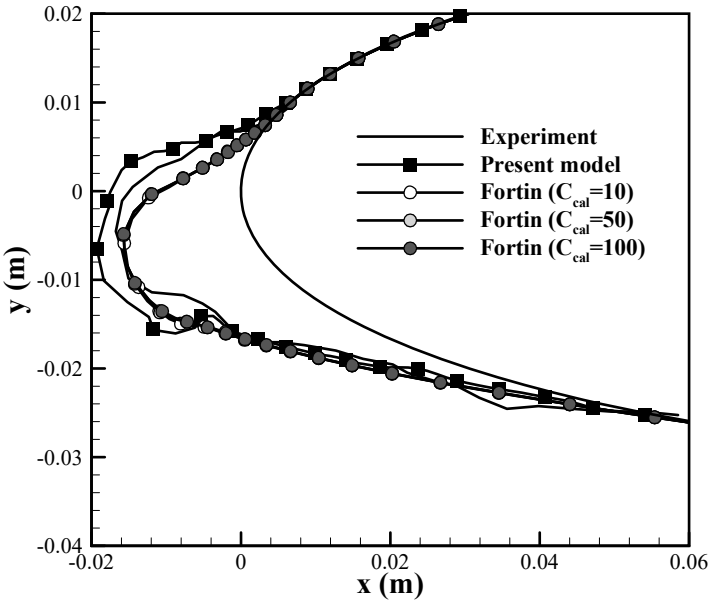

(b) Rime case

Figure 2. Ice shape variation due to C_{cal}

Fig 3 presents the effect of C_{cal}. Fig 3(a) shows the change in the roughness height according to the change in C_{cal}, and Fig 3(b) shows the change in h_{cv}. As C_{cal} increases, the roughness height and h_{cv} increase. The variation in the roughness height and h_{cv} significantly depends on the change in C_{cal}, which affects the ice shape. However, because the current model does not employ this arbitrary variable, it predicts the shape uniformly. This is owing to the difference in the aerodynamic solver used in each code. In contrast with the Navier–Stokes solver-based code, the panel method used in Fortin's model does not provide all the parameters needed for the model, such as wall shear stress. Therefore, to consider these values additionally, an analytical model called the boundary layer theory is used. Subsequently, C_{cal} is used to match the numerically calculated ice shape to the experimental result. In this study, the arbitrariness of the solution of the previous model is avoided.

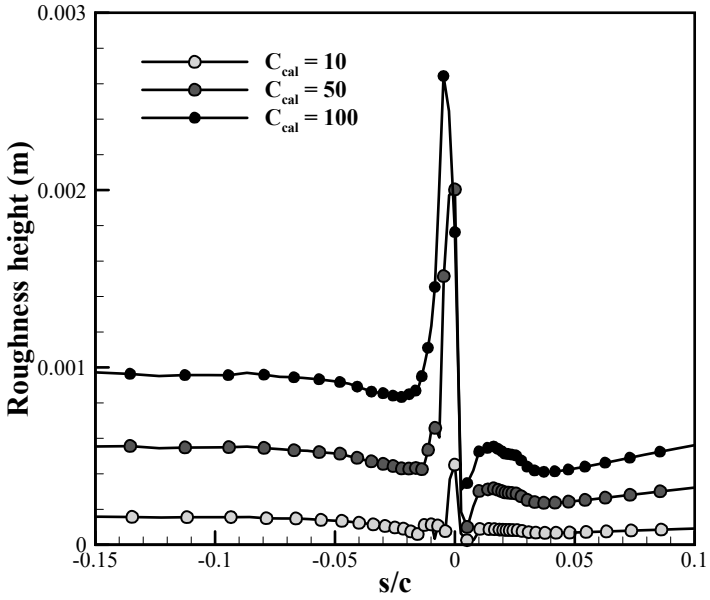

(a) Roughness height

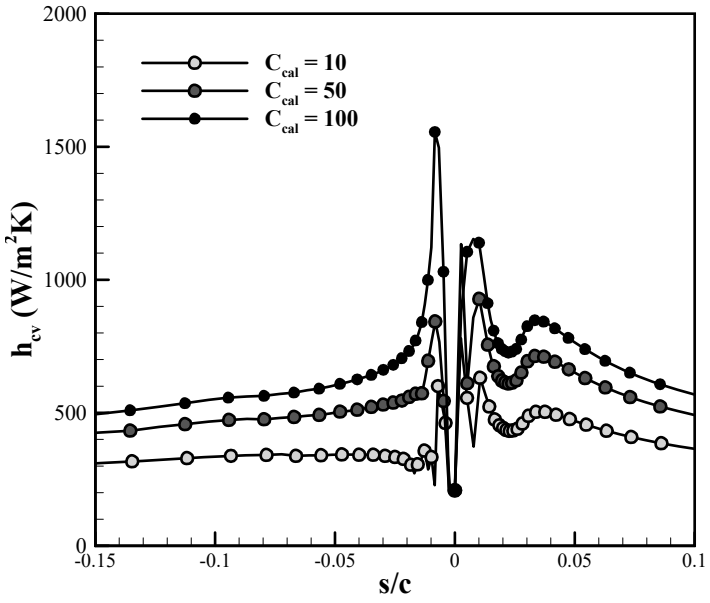

(b) h_{cv}

Figure 3. Effect of C_{cal} on the roughness height and h_{cv}

3.3 Ice shape verification – NASA empirical correlation

The NASA empirical correlation is determined by comparing the experimental and simulation profiles at three airspeeds, four LWCs, and four temperature conditions. The velocity covers most of the experimental range tested by NASA, but the LWC is between 0.25 and 1.0, which is unsuitable for high-LWC cases. In addition, the temperature range is from -8 °C to -22 °C, under which conditions the glaze ice is less. [2] This does not include the condition near the freezing point where glaze ice generally appears.

Fig 4 compares the ice shapes under the conditions for which the NASA empirical correlation is derived. No significant difference is observed between the results of the current model and empirical correlation, whereas some deviation is noted from the experimental results. Fig 5 presents the roughness height and heat convection energy difference obtained with the model application. Table 3 summarizes the conditions for the comparison.

Table 3. Empirical correlation conditions for comparison [13]

Case	Airspeed (m/s)	Temperature (°C)	LWC (g/m^3)	MVD (μm)	Time (s)
A	102.8	-11.1	0.55	20	360
B	102.8	-9.71	0.55	20	360

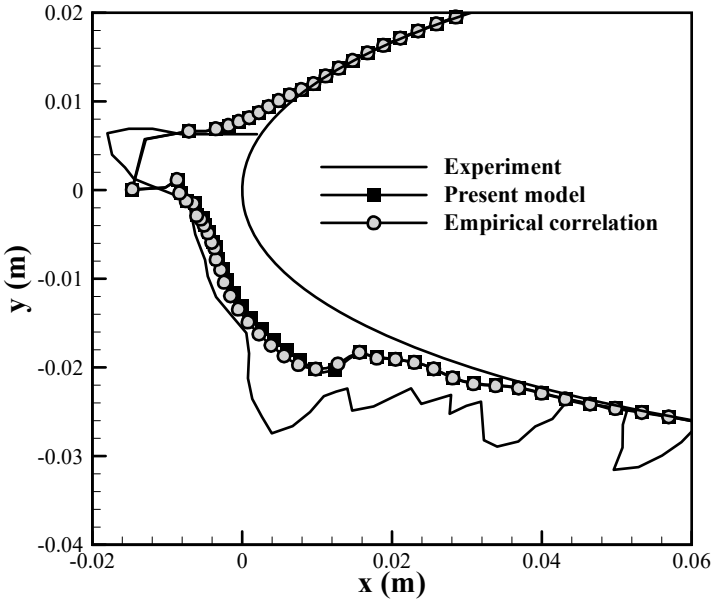

(a) Ice shape for case A

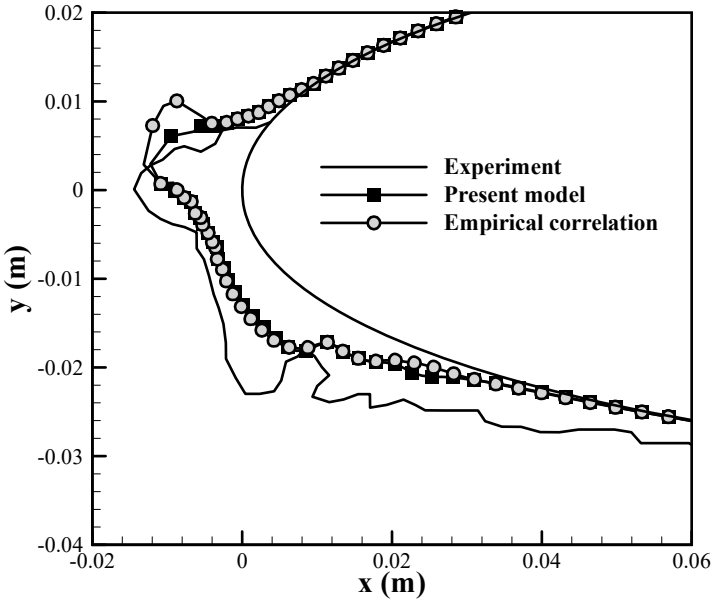

(b) Ice shape for case B

Figure 4 Ice shape under different conditions

The present roughness model computes the local roughness height from the surface, as shown in Fig 5(a). Near the stagnation point, the collection efficiency is high, and a water film is formed owing to the high-impinging water mass. In this smooth zone, a low roughness height is predicted. In contrast, on moving to the trailing edge, the remaining water mass decreases, and the rivulet and bead appear to exhibit a large roughness height. Particularly on the upper surface, the bead height is greater owing to the aerodynamic force with a strong favorable pressure gradient.

Fig 5(b) displays the heat convection energy difference when applying the roughness models. In contrast with the difference in the roughness height in the smooth zone, the heat convection energy difference is below 10% and there is no significant difference in the ice shape. Currently, the effect of surface roughness is shown only by the enhancement of the thermal conductivity with the present aircraft icing code. Therefore, in the present conditions, the results of the empirical correlation and current model are similar.

Fig 6 compares the ice shapes of the current model with those of the empirical correlation under different empirical correlation conditions. In Fig 6(a), high-temperature and high-LWC results are displayed, whereas Fig 6(b) corresponds to only high LWC. The conditions are specified in Table 4.

Table 4. Empirical correlation conditions for comparison [13]

Case	Airspeed (m/s)	Temperature (°C)	LWC (g/m^3)	MVD (μm)	Time (s)
C	58.1	-2.91	1.30	20	360
D	102.8	-11.15	1.30	20	360

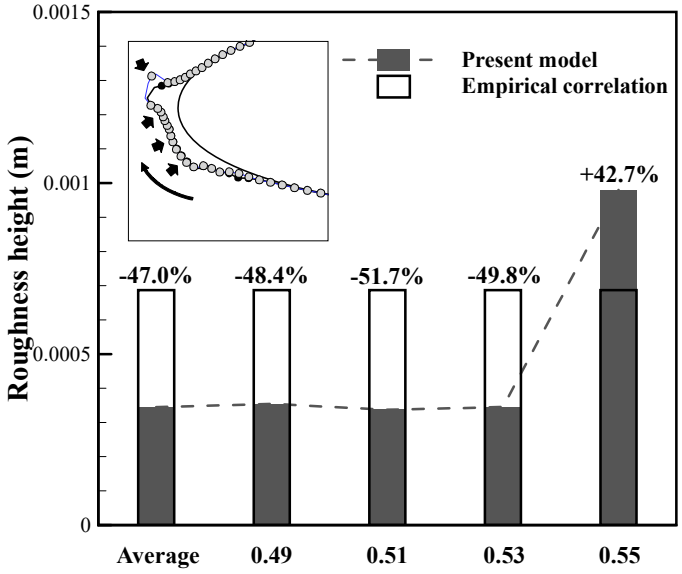

(a) Roughness height distribution

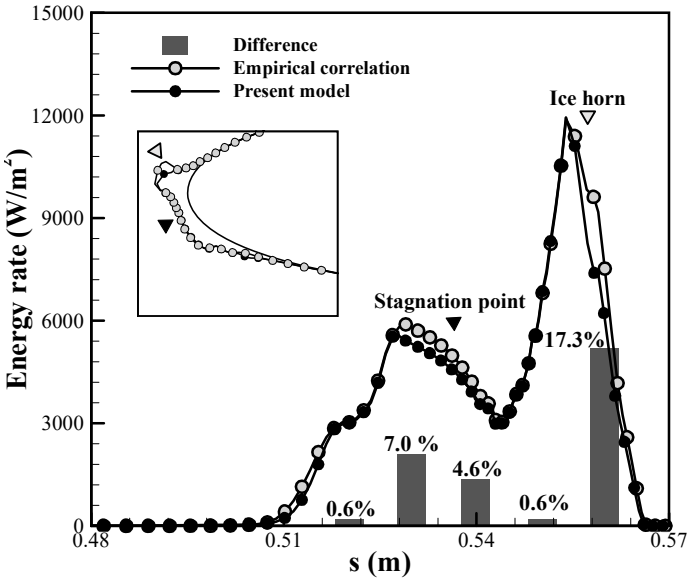

(b) Convection energy distribution

Figure 5. Comparison of the roughness height and convection energy distribution

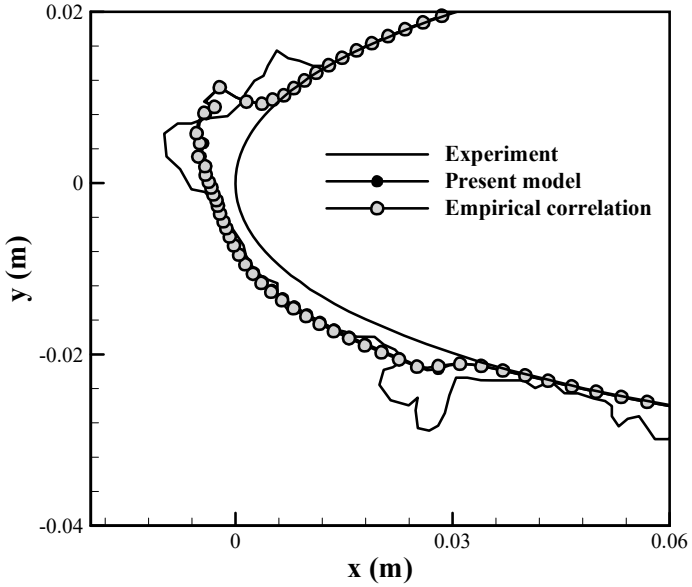

(a) Ice shape for case C

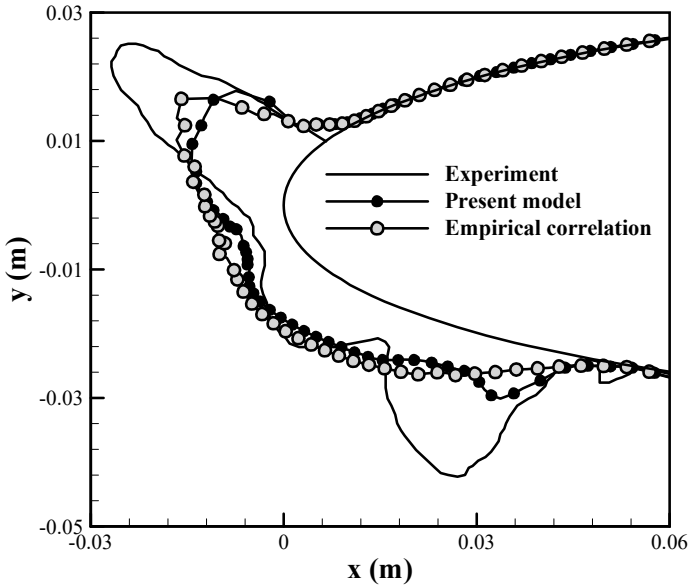

(b) Ice shape for case D

Figure 6 Ice shape comparison at different empirical correlation conditions

Fig 6(a) does not exhibit a significant shape change because the surface temperature is similar to the ambient temperature, and the heat convection is small even though the surface roughness changes abruptly. In contrast, Fig 6(b) is the result of low-temperature and high-LWC conditions, and the ice shape with the empirical correlation is different from the experiment. The empirical correlation predicts a high roughness owing to the high LWC, and computes a higher heat convection and thickness. Specifically, near the stagnation point where a smooth zone appears owing to the water film, excessive ice is predicted. Thus, it does not accurately exhibit the ice horn, an important feature of performance degradation. Because the local roughness height is distinguished by the present model, the ice shape has a similarity with the experimental result.

In summary, because the empirical correlation predicts the roughness height by extrapolating the existing results, it predicts a much higher roughness height and h_{cv}, resulting in concentrated ice accretion locally. The roughness height is partly calculated when the current model is applied, and the ice shape indicates an improved feature. However, for all the cases, the numerical results underestimate the ice shape, particularly for a smaller surface. The thermodynamic model currently used in the numerical simulations predicts ice shapes from a macroscopic point of view based on the mass conservation and energy conservation relations with a controlled volume. However, according to a previous observation regarding the ice accretion process, the roughness element is responsible not only for the heat convection enhancement, but also for the microscopic motion, which the current numerical method does not model, such as the increase in the local collection efficiency. Therefore, a study on simulating the effect of surface roughness is required.

3.4 Further studies

In this study, by applying the physical model for roughness prediction on the surface, the roughness height, heat convection and shape were obtained to compare with the numerical result with empirical roughness prediction. Taken together, the above results show that the surface roughness height obtained by the current method is generally less than the value obtained by the empirical equation. Similarly, the heat transfer coefficient and the ice accretion rate tend to predict less. This model predicts the physically valid values as a whole, while the existing empirical correlation predicts excess surface roughness except for certain conditions. Also, by minimizing the use of empirical parameters, we also reduced the randomness of the results. However, the present model shows a tendency that the surface roughness value and shape are smaller than the experimental value. This discrepancy is due to some errors in the assumptions on which the current model is based.

First, the current model calculates the surface roughness based on the equilibrium equations of force for water on the surface. This hypothesis is valid considering that the glaze region coexists with water and ice. However, for the rime region where the droplet freezes at the same time with impingement of the droplet, roughness elements are defined by the initially formed roughness by the frozen droplets. From the experiment conducted by McClain and Vargas[15], the roughness variation along the surface of iced airfoil was scanned and captured, concluding that while liquid film physics is important to the glaze region, ice roughness value at the rime ice region is affected by the collection efficiency.

Secondly, the current model limits the effect of surface roughness on the flow field to the effect inside the boundary layer through the turbulence model. Since RANS-based numerical analysis is currently used, the surface roughness does not appear directly in the shape but is considered as an element that influences the flow or thermodynamic properties during calculation. For this reason, the simulation result does not show the surface roughness of macro scale like the feather shape on the bottom surface that appears from the actual experimental results. However, such a high surface roughness height affects the droplet trajectory as well as the flow characteristics of the turbulent flow, and accordingly, the ice accretion mass is increased occurring some discrepancy of ice accretion in the suction side between the numerical results and the experimental results. It is not reasonable to reflect this effect in the turbulence model if the height of the generated surface roughness is larger or not different from the thickness of the boundary layer. Some experiments have addressed the need for further consideration of this assumption. Shin[5] analyzed the roughness height, boundary layer thickness and the critical roughness height, and remarked that the relationship between macro surface irregularity and the micro roughness need to be accounted for not just by the roughness model.

To sum up with, considering that the current model is based on the force equilibrium equations for the physics of the water film, the surface roughness prediction in the glaze region is based in reasonable physical basis. However, physics is not properly modeled for rime ice regions and transition regions where feather-shaped roughness occurs after the glaze region. Therefore, a new numerical model is needed for the transition and rime ice regions, not just the liquid film based roughness model.

4. Conclusions

This study proposes an improved surface roughness model for application in an aircraft icing code based on the Navier–Stokes equation. The concept of the model was to distinguish three surface states based on the film thickness and to compute the roughness height. For the implementation of the model with a quasi-steady state solver, a new analytical model derived from the governing equation of the thermodynamic module was introduced. The proposed methodology was verified by other roughness models. The findings of the study are as follows:

1) By extending the present model to the Navier–Stokes solver, the arbitrariness due to the limitations of the panel method used in the previous roughness model was removed. Not all the parameters required for the roughness model are provided with the panel method, and the analytical models that are used lower the fidelity of the solver. Therefore, C_{cal} is applied to correct the roughness height by matching the numerically calculated ice shape with the experiment. The current model excluded the arbitrariness by proposing an analytical model derived from the governing equation of the thermodynamic model.

2) The results from the empirical correlation predicted the ice shapes well for conditions similar to those derived for the correlation. Beyond these conditions, the current model showed improved shape characteristics compared with the empirical correlation. This tendency was exhibited particularly at high-LWC and low-temperature conditions because the empirical corrections calculated the surface roughness excessively.

Along with the advances in the methodology, this study showed the limitations of the existing models, and in some cases, it predicted an improvement in the ice shape. It was confirmed that the physical model for the roughness height was reliable, and the empirical parameters were eliminated to be applied to the Navier–Stokes solver-based aircraft icing code. However, there were some limitations of implementing this model alone to the icing code to predict the surface roughness. Because the effect of surface roughness was not fully considered, except for the heat convection enhancement, further investigation is required for accurate calculations. Nevertheless, this study has laid the basis for a heuristic approach for a more advanced modeling based on physical phenomena.

References

[1] Ruff, G. A., and Berkowitz, B. M., "Users' Manual for the NASA Lewis Ice-Accretion Prediction Code (LEWICE)," NASA CR 185129, May 1990.

[2] Gent, R., Markiewicz, R., and Cansdale, J., "Further studies of helicopter rotor ice accretion and protection," *Vertica*, Vol. 11, 1987, pp. 473-492.

[3] Olsen, W., and Walker, E. "Experimental Evidence for Modifying the Current Physical Model for Ice Accretion on Aircraft Surfaces," NASA TM 87184, May 1986.

[4] Hansman, R. J,. and Turnock, S. R., "Investigation of Surface Water Behavior During Glaze Ice Accretion," *Journal of Aircraft*, Vol. 25, No. 2, 1989, pp.140-147.

[5] Shin, J., "Characteristics of Surface Roughness Associated with Leading Edge Ice Accretion," NASA TM-106459, Jan 1994.

[6] Beysens, D., "The formation of dew", *Atmospheric research*, Vol. 39, Issues 1-3, 1995, pp. 215-237.

[7] Fortin, G., Laforte, J.-L., and Ilinca, A., "Heat and Mass Transfer during Ice Accretion on Aircraft Wings with an Improved Roughness Model", *International Journal of Thermal Sciences*, Vol. 45, Issue. 6, 2006, pp. 595-606.

[8] Croce, G., De Candido, E., Habashi, W. G., Munzar, J., Aubé, M. S., Baruzzi, G. S., and Aliaga, C., "FENSAP-ICE: Aanalytical Model for Spatial and

Temporal Evolution of In-flight Icing Roughness," *Journal of Aircraft*, Vol. 47, No. 4, 2010, pp. 1283–1289.

[9] OpenFOAM, "Open-source Field Operation and Manipulation," Software Package, Ver. 2.2.0, 2011, http://www.openfoam.com.

[10] Aupoix, B., and Spalart, P. R., "Extension of the Spalart-Allmaras Turbulence Model to Account for Wall Roughness," *International Journal of Heat and Fluid Flow*, Vol. 24, No. 4, 2003, pp. 454–462.

[11] Son, C., Oh, S., and Yee, K., "Ice Accretion on Helicopter Fuselage Considering Rotor-Wake Effects," *Journal of Aircraft*, Vol. 54, No. 2, 2017, pp. 500–518.

[12] Messinger, B. L., "Equilibrium Temperature of an Unheated Icing Surface as a Function of Air Speed," *Journal of the Aeronautical Sciences*, Vol. 20, No. 1, 1953, pp. 29–42.

[13] Wright, W. B., and Rutkowski, A., "Validation Results for LEWICE 2.0," NASA CR-1999-208690, Jan 1999.

[14] Al-Khalil, K. M., T. G. Keith Jr, and K. J. De Witt. "Further development of an anti-icing runback model." 29th Aerospace Sciences Meeting & Exhibit, AIAA-91-0266, 1991, pp. 12.

[15] S. T. McClain, M. Vargas and J. Tsao, "Characterization of ice roughness variations in scaled glaze icing conditions," 8th AIAA Atmospheric and Space Environments Conference, June. 2016. P. 3592.